Applied Physics Letters

Tunable magnetoresistance and thermopower in interconnected NiCr and CoCr nanowire networks

Cite as: Appl. Phys. Lett. **115**, 242402 (2019); https://doi.org/10.1063/1.5130718
Submitted: 07 October 2019 . Accepted: 20 November 2019 . Published Online: 09 December 2019

Tristan da Câmara Santa Clara Gomes, Nicolas Marchal, Flavio Abreu Araujo, and Luc Piraux

Applied Physics Letters ARTICLE scitation.org/journal/apl

Tunable magnetoresistance and thermopower in interconnected NiCr and CoCr nanowire networks

Cite as: Appl. Phys. Lett. **115**, 242402 (2019); doi: 10.1063/1.5130718
Submitted: 7 October 2019 · Accepted: 20 November 2019 ·
Published Online: 9 December 2019

Tristan da Câmara Santa Clara Gomes, Nicolas Marchal, Flavio Abreu Araujo, and Luc Piraux[a)]

AFFILIATIONS

Institute of Condensed Matter and Nanosciences, Université catholique de Louvain, Place Croix du Sud 1, 1348 Louvain-la-Neuve, Belgium

[a)]Electronic mail: luc.piraux@uclouvain.be

ABSTRACT

Magnetoresistance and thermopower of crossed NiCr and CoCr nanowire networks have been measured as a function of temperature and chromium content in dilute alloys. At low temperatures, it is found that the impurity effect leads to negative anisotropic magnetoresistance, an observation that even persists until room temperature in diluted CoCr alloy nanowires. The addition of a small amount of Cr in nickel nanowires also abruptly reverses the sign of the thermopower from $-20\ \mu$V/K for pure Ni up to $+18\ \mu$V/K for the dilute alloys, implying the switching from n- to p-type conduction. These results are consistent with pronounced changes in the density of states for the majority spin electrons. The high room-temperature power factors of these magnetic nanowire networks (in the range of 1–10 mW/K^2 m) provide interesting perspectives for designing n- and p-type legs for flexible spin thermoelectric devices.

It has been found that the addition of transition metal impurities in 3d ferromagnetic metals has a considerable impact on their spin-dependent electronic transport properties (for a review, see Ref. 1). The effects can be understood in terms of matching/mismatching of the d-electronic states between impurities and host metal.[2] In particular, Cr impurities in Co, Fe, and Ni produce stronger scattering in the majority-spin channel in a two-band model, which makes the spin-asymmetry parameter $\alpha = \rho_\downarrow/\rho_\uparrow$, where $\rho_\downarrow$ ($\rho_\uparrow$) is the resistivity for the majority (minority) spin electrons, less than unity and thus opposite to that in pure ferromagnetic metals. Phenomena such as negative anisotropic magnetoresistance (AMR) effects have been reported in diluted NiCr alloys at low temperature.[3–5] In addition, ferromagnetic metals may exhibit large Seebeck coefficients S because of the pronounced structure of the d-band and the high-energy derivative of the density of states (DOS) at the Fermi energy.[6] Besides, the thermopower for spin up and spin down electrons is different due to the exchange splitting of their bands and the significant difference between the majority-spin DOS and minority-spin DOS near the Fermi level, as suggested from previous works performed on dilute magnetic alloys.[7,8] Also, the room-temperature (RT) Seebeck coefficient has been observed to change its sign in some dilute magnetic alloys, e.g., S is negative for pure Ni ($S = -20\ \mu$V/K) and positive for NiCr alloys with 2–3 at. % Cr ($S \approx +20\ \mu$V/K).[8] These effects are also related to the drastic change in the DOS at the Fermi level by the incorporation of Cr impurities in ferromagnetic metals. More recently, thermoelectric effects in spintronic materials are actively studied in the emerging field of spin caloritronics, giving rise to interesting physical phenomena and functionalities in the existing thermoelectric technology.[9–12] In this context, the thermoelectric analogs of the magnetoresistive effects in magnetic multilayers and in magnetic tunnel junctions such as the giant magneto-Seebeck and magneto-Peltier exploit the fact that the Seebeck and Peltier coefficients for spin-up and spin-down electrons are significantly different. A magnetic approach to control the thermoelectric properties is of great relevance to enable active modulation of both heat flow and thermoelectric voltages for waste-heat recovery from electronic circuits.[11,13–15] Also, there is a significant challenge to fabricate flexible thermoelectric materials and generators that are attractive for applications in thermal energy harvesting as a means to power wireless sensors and portable wearable electronic devices.[16–18]

To this end, it was recently demonstrated that interconnected magnetic nanowire (NW) networks fabricated by electrochemical deposition in 3D nanoporous polymer host films provide an attractive pathway to fabricate light, robust, flexible, and shapable spin caloritronic devices in versatile formats that meet key requirements for electrical, thermal, and mechanical stability.[19,20] In addition, electrochemical synthesis is a powerful method for fabricating multicomponent nanowires with different metals due to its engineering simplicity, versatility, and low-cost.[21,22] The conventional thermoelectric modules consist of coupled n- and

p-type thermoelectric materials or legs. Recent research has focused on the spin-dependent thermoelectric properties of n-type NW systems.[19,20,23] These magnetic nanowires were found to exhibit a very high thermoelectric power (TEP) factor up to 7.5 mW/K^2 m at room temperature, which are larger values than the power factor of the widely used thermoelectric material, bismuth telluride (in the range of 1–5 mW/K^2 m).[24] In this work, we demonstrate the fabrication of nanowire networks based on diluted NiCr and CoCr alloys by electrochemical deposition in 3D porous membranes. The influence of the impurity concentration on the magnetoresistance (MR) and thermoelectric power (TEP) is investigated. Both negative anisotropic magnetoresistance (AMR) at RT and tunable Seebeck coefficients have been observed. The results obtained on dilute NiCr alloys are promising for the fabrication of flexible p-type nanowire based thermoelectric legs.

Polycarbonate (PC) porous membranes with interconnected pores have been fabricated by exposing a 22 μm-thick PC film to a two-step irradiation process.[25,26] The topology of the membranes was defined by exposing the film to a first irradiation step at two fixed angles of $-25°$ and $+25°$ with respect to the normal axis of the film plane. After rotating the PC film, in the plane by 90°, the second irradiation step took place at the same fixed angular irradiation flux to finally form a 3D nanochannel network. Then, the latent tracks were chemically etched following a previously reported protocol[27] to obtain 3D porous membranes with pores of 80 nm diameter and a volumetric porosity of 3%. Next, the PC templates were coated on one side using an e-beam evaporator with a metallic Cr (3 nm)/Au (400 nm) bilayer to serve as a cathode during the electrochemical deposition. The NW network partially fills the 3D porous PC membrane, typically in the range of 30%–70% of the total pore volume. Pure Ni and Co NW networks were synthesized from electrolyte solutions composed of 1 M $NiSO_4 \cdot 6H_2O + 0.5$ M H_3BO_3 and 0.85 M $CoSO_4 \cdot 7H_2O + 0.5$ M H_3BO_3, respectively. The pH acidity of the Co-based solution was lowered to 2 to avoid any magnetocrystalline anisotropy.[28] Deposition potentials of -1.1 and -0.95 V were used for the electrodeposition of Ni and Co NWs, respectively. Interconnected NiCr alloy NWs (Cr content ≤ 7 at. %) were obtained by adding between 1 and 5 mM of $CrCl_3 \cdot 6H_2O$ into an electrolyte solution containing 60 mM of $NiSO_4 \cdot 6H_2O$ and 0.5 M H_3BO_3. Dilute CoCr alloy NW networks with a Cr content ≤ 5 at. % were grown by adding between 10 and 50 mM of $CrCl_3 \cdot 6H_2O$ into an electrolyte solution containing 1 M $CoSO_4 \cdot 7H_2O$ and 0.5 M H_3BO_3. The deposition potential was -1.2 V for both NiCr and CoCr dilute alloy NWs. The interconnected NW structure embedded into the PC template is schematically represented in Fig. 1(a). In order to perform MR and TEP measurements, the cathode was locally removed by plasma etching to form a two-probe electrode system, as shown in Figs. 1(b)–1(d). For TEP measurements, heat flow is generated by a resistive element and a thermoelectric voltage ΔV is created by the temperature difference ΔT between the two metallic electrodes that is measured by a thermocouple (see Ref. 19 for details). MR and TEP were measured at temperatures from 10 to 300 K. For MR measurements, the external magnetic field was applied along the out-of-plane (OOP) and in-plane (IP) directions of the NW network films. The interconnected NW structure was characterized using a field-emission scanning electron microscope (FE-SEM) after chemical dissolution of the PC template. The various interconnected NW networks were found to be mechanically stable and self-supported, as illustrated by the SEM image shown in Fig. 1(e). X-ray spectroscopy (EDX) has provided the chemical composition of the NiCr and CoCr dilute alloy NWs, expressed as atomic percentage in this work. We observed that the Cr content increased almost linearly with respect to the concentration of $CrCl_3 \cdot 6H_2O$ added to the solution, which allows us to adjust precisely the Cr content into the alloy NW networks. MR and TEP measurements were performed on NiCr alloys with Cr 2–7 at. % and CoCr alloys with Cr 1–5 at. %.

Figures 2(a)–2(c) show the RT resistance curves as a function of the magnetic field applied in the IP and OOP directions for Ni, $Ni_{98}Cr_2$, and $Ni_{96}Cr_4$ NW networks. The results correspond well to the AMR effect, which reflect resistivity variation as the angle between the magnetization and current directions is modified. Here, the MR ratio is defined as $MR = (R_{OOP} - R_{IP})/R_{OOP}$, with R_{OOP} and R_{IP} being the resistance states in the OOP and IP directions at $H = 10$ kOe, respectively. Note that the MR ratio is smaller than the AMR defined as $(R_{\parallel} - R_{\perp})/R_{\perp}$, with $R_{\parallel}$ and $R_{\perp}$ being the theoretical resistance states for the parallel and perpendicular configurations between magnetization and current, respectively. Indeed, with the current flow being restricted along the NW segments, the saturation magnetization in the OOP direction makes an average angle of $\pm 25°$ with the current. Also, when the magnetization is saturated in the IP direction, the average angle between the magnetization and the current flow is $\pm 65°$. In a previous work,[28] an analytical model inherent to the

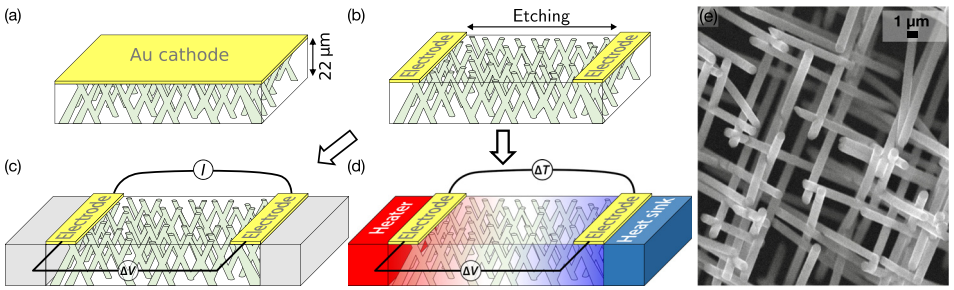

FIG. 1. 3D interconnected nanowire networks and experimental measurements setups. (a) Schematic of the 3D interconnected nanowire network film grown by electrodeposition from a Au cathode into a polycarbonate template with crossed-nanopores. (b) Two-probe electrode design obtained by local etching of the Au cathode. [(c) and (d)] Device configuration for successive measurements of the magnetoresistance effect and the Seebeck coefficient. Heat flow in (d) is generated by a resistive element, and a thermoelectric voltage ΔV is created by the temperature difference ΔT that is measured by a thermocouple. (e) Low-magnification SEM image of the self-supported interconnected Ni nanowire (NW) network showing the top view of the NW network with an 80 nm diameter and a 3% packing density.

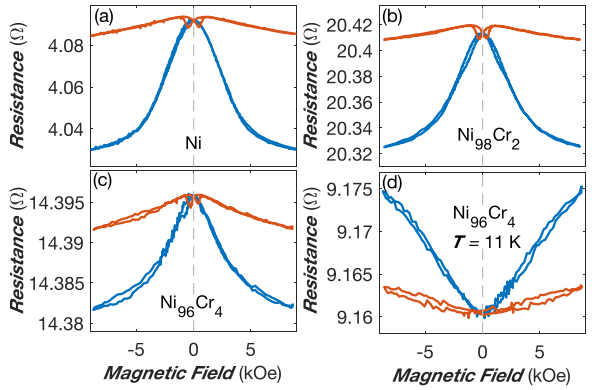

FIG. 2. Magnetoresistive curves of interconnected Ni and NiCr nanowire networks. [(a)–(c)] Room-temperature magnetoresistive curves with the applied magnetic field along the out-of-plane (red) and in-plane (blue) directions for the Ni crossed nanowire network (a) and for NiCr crossed nanowire networks with Cr contents of 2% (b) and 4% (c), respectively. (d) Magnetoresistive curves for the sample in (c) at $T = 10$ K.

topology of 3D nanowire networks has been proposed to extract the AMR ratios from the measured resistance values at saturation R_{OOP} and R_{IP}. However, the case $R_{OOP} > R_{IP}$ unambiguously reflects a positive AMR effect, which is usually observed in ferromagnetic metals and alloys. In spite of the decrease in amplitude of AMR when adding the Cr content, a similar behavior is observed at RT for the various NiCr alloy NWs. In contrast, the sign of the AMR ratio changed from positive to negative when the temperature is reduced, as illustrated in Fig. 2(d), where resistance curves obtained at $T = 10$ K are reported for the $Ni_{96}Cr_4$ sample. Negative AMR at low temperature was also observed on the other NiCr NW samples. These observations are in agreement with previously reported measurements in bulk NiCr dilute alloys.[3–5]

Figures 3(a)–3(c) show the MR curves obtained for Co, $Co_{99}Cr_1$, and $Co_{95}Cr_5$ NW networks at RT. As shown in Figs. 3(a) and 3(b), the AMR is positive in both Co and $Co_{99}Cr_1$ NWs. In contrast,

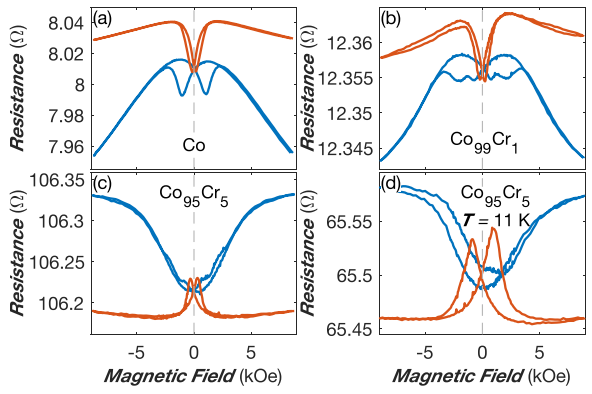

FIG. 3. Magnetoresistive curves of interconnected Co and CoCr nanowire networks. [(a)–(c)] Room-temperature magnetoresistive curves with the applied magnetic field along the out-of-plane (red) and in-plane (blue) directions for the Co crossed nanowire network (a) and for CoCr crossed nanowire networks with Cr contents of 1% (b) and 5% (c), respectively. (d) Magnetoresistive curves for the sample in (c) at $T = 10$ K.

interconnected $Co_{95}Cr_5$ NW networks exhibit the opposite behavior where $R_{IP} > R_{OOP}$, as shown in Fig. 3(c). A similar behavior was found for the interconnected $Co_{97}Cr_3$ NW network (not shown in Fig. 3). While negative AMR at RT was previously observed in CoIr,[29] such an effect has not been reported before in dilute CoCr alloys. A similar negative AMR effect is observed at low temperature for the $Co_{95}Cr_5$ NW network, as shown in Fig. 3(d). Even if the interpretation is still controversial,[29] the sign of the AMR ratio has been tentatively linked to the value of the spin asymmetry coefficient $\alpha = \rho_\downarrow/\rho_\uparrow$ in the alloy through a model based on a spin–orbit mechanism.[4,30] The model proposed by Campbell, Fert, and Jaoul predicts that at low temperatures, the AMR is proportional to the quantity $(\alpha - 1)$, and so a negative AMR ratio is expected when electronic conduction is dominated by minority spin electrons, i.e., $\alpha < 1$. In this simplified model, the value of α is fixed for a given impurity and independent of the concentration. However, at higher temperatures, additional terms must be added in the resistivity due to electron–phonon and electron–magnon scattering processes and the values of the AMR ratio for dilute alloys should tend to that of the pure metal, converging faster as their concentrations are lower.[30] These results on dilute NiCr and CoCr NW networks are consistent with a spin asymmetry coefficient $\alpha < 1$, as predicted theoretically.[1,31]

The evolution of the MR ratio with respect to the Cr content for NiCr NW networks is shown in Fig. 4(a) at RT and $T = 100$ K. For all samples, positive values are found at RT, showing a rapid decrease in MR with the increasing Cr concentration. In contrast, the negative MR ratio was measured at $T = 100$ K for the NiCr sample with 4 and 7 at. % of Cr. The inset in Fig. 4(a) shows the temperature variation of the MR ratio for the interconnected $Ni_{96}Cr_4$ NW network. As observed, the MR ratio gradually increases from its negative value at low

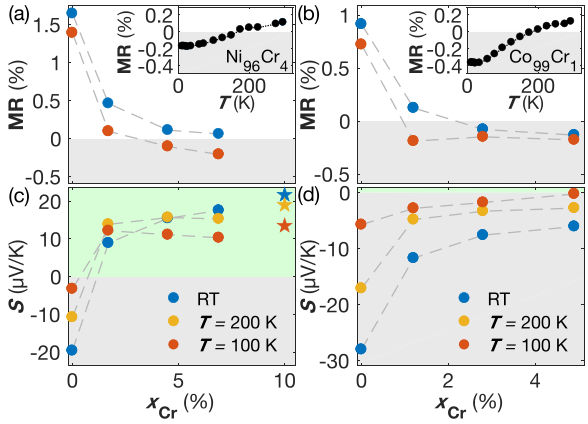

FIG. 4. Anisotropic magnetoresistance and Seebeck coefficient of NiCr and CoCr NW networks vs Cr content at different temperatures. [(a) and (b)] MR ratio vs the Cr content for NiCr (a) and CoCr (b) samples at room-temperature (blue) and $T = 100$ K (red). The inset in (a) shows the MR ratio of the NiCr sample with 4% of Cr as a function of temperature, while the inset in (b) shows the MR ratio of the CoCr sample with 1% of Cr as a function of temperature. The gray areas in (a) and (b) indicate negative AMR. (c) and (d) Seebeck coefficient vs Cr content of NiCr (c) and CoCr (d) samples at room temperature (blue), $T = 200$ K (yellow), and $T = 100$ K (red). The data were obtained at zero magnetic field. The star symbols correspond to the recommended values for chromel ($Ni_{90}Co_{10}$) The green and gray areas in (c) and (d) indicate p- and n-type thermoelectric effects, respectively. The symbol size encompasses the experimental error bars.

temperature to positive values for $T > 150$ K. In contrast, CoCr alloy NWs display negative AMR at RT for a Cr concentration ≥ 3 at. %. Negative values are also obtained at $T = 100$ K for all CoCr NW samples, and the absolute values for MR at low temperatures are almost independent of the alloy content even for a Cr concentration as small as ~1 at. %. The inset of Fig. 4(b) shows the gradual change in the sign of MR(T) for the sample with the lower Cr concentration ($Co_{99}Cr_1$). The MR changes from negative to positive values at $T = 175$ K. Overall, the model predictions of Campbell *et al.*[4,30] are in qualitatively good agreement with the experiments performed on both NiCr and CoCr alloy NW networks. In particular, the experimental results obtained at low temperature on CoCr NWs follow the prediction of MR being independent of the impurity concentration. The change of sign at RT favored for the lowest Cr concentrations constitutes another experimental evidence. However, the fact that the negative MR in $Co_{97}Cr_3$ and $Co_{95}Cr_5$ NW networks remains almost unchanged between $T = 100$ K and RT is unexpected since scattering of conduction electrons at RT should significantly weaken the effect, a problem already pointed out in earlier studies performed on bulk CoIr alloys.[29]

Figures 4(c) and 4(d) show the variation of the Seebeck coefficient with the Cr content at some selected temperatures in the absence of any external magnetic field for the interconnected NiCr and CoCr NW networks. As shown in Fig. 4(c), the thermopower of NiCr suddenly changes sign from negative to relatively large positive values with the addition of Cr impurities in Ni. The RT Seebeck coefficient goes from $-20\,\mu$V/K to about $+17.5\,\mu$V/K for the NiCr alloys with 7 at. % of Cr. Similar changes in thermopower sign have been reported in bulk NiCr alloys where minority spin dominates the electrical conduction.[1,7,8] The sign inversion of the Seebeck coefficient from negative to positive in dilute NiCr alloys could be explained on the basis of a virtual bound state passing through the Fermi level in the spin up band.[7,8] For comparison, the tabulated data for the thermocouple material Chromel P ($Ni_{90}Cr_{10}$) are also included in Fig. 4(c). These results are in very reasonable agreement with our own values. In addition, extremely small magnetothermopower effects were found in our samples (typically less than 1%). Using the residual resistivity ratio ($R_{290\,K}/R_{10\,K}$) and reported RT resistivity for the thermally excited scatterings (phonons and magnons) for the NiCr alloys,[32] the RT power factors ($PF = S^2/\rho$, with ρ being the electrical resistivity) have been estimated to be 4.2 and 0.9 mW/K^2 m for the Ni and $Ni_{96}Cr_4$ NW networks, respectively. Since the power factor of $Ni_{96}Cr_4$ NW networks is similar to that of widely used thermoelectric material bismuth–telluride (in the range of 1–5 mW/K^2 m) and only slightly lower than the largest room-temperature PF value for p-type thermoelectric materials (PF $\approx$ 9 mW/K^2 m for $CePd_3$[33]), such electrodeposited NiCr NW networks are suitable as p-type thermoelectric materials. Because of the very low thermal conductivity of polycarbonate ($\kappa = 0.2$W/m · K at RT), the contribution of the polymer matrix to heat transport is much smaller than that of the metallic NW network. For metallic NWs, heat transport is dominated by the electron heat conduction flux, and so assuming that the Wiedemann–Franz law holds the figure of merit is reduced to $ZT = S^2/L_0$, with L_0 being the Lorenz number. Using this approximation, we obtain $ZT = 1.6 \times 10^{-2}$ and $ZT = 1.3 \times 10^{-2}$ at RT for the Ni and $Ni_{96}Cr_4$ NW networks, respectively. Although the ZT values in these NW networks are almost two orders of magnitude smaller than those in BiTe alloys, they are comparable to those of thermocouple alloys ($ZT = 6 \times 10^{-2}$ and $ZT = 1.4 \times 10^{-2}$ in constantan and chromel, respectively). In contrast, the sign of the Seebeck coefficient does not change for any value of Cr concentration for CoCr NW networks [see Fig. 4(d)]. The RT thermopower drops rapidly from $-28\,\mu$V/K for pure Co to much smaller negative values approaching $-5\,\mu$V/K for $Co_{95}Cr_5$ NWs. The CoCr NW samples are found to exhibit the same features at lower temperatures, as also shown in Fig. 4(d). Although the thermopower of bulk CoCr alloys was not reported as far as we know, the results obtained on CoCr NWs are consistent with the data previously obtained on dilute Co-based alloys such as CoV, CoMo, and CoRe alloys,[6] in which $\alpha < 1$ is expected. The sudden drop of S caused by 1%–5% Cr addition to Co NWs should also be related to pronounced changes in the density of states for the majority spin electrons. Besides, the Co NW networks have been found to exhibit large PF at a RT of about 11.0 mW/K^2 m, which is close to the largest RT power factor achieved in bulk Co (PF $\approx$ 15 mW/K^2 m),[14] making them suitable for n-type thermoelectric legs.

In conclusion, interconnected NiCr and CoCr nanowire networks were synthesized on a large scale by direct electrodeposition in polymer membranes with crossed cylindrical nanopores allowing fine-tuning of the alloy composition. The magnetoresistance and thermopower properties have been investigated as a function of temperature for various alloy compositions in the range of 1–7 at. % Cr. Negative anisotropic magnetoresistance was observed at low temperatures in both NiCr and CoCr NW networks. The magnetoresistance remains negative at room temperature for CoCr alloy NWs with a Cr concentration ≥ 3 at. %. The observed negative magnetoresistance characteristics denote expected behavior for an electrical conduction dominated by minority spin electrons. The possibility to change the Seebeck coefficient sign has also been evidenced in NiCr NW networks. The room temperature thermopower changes abruptly from negative ($-20\,\mu$V/K) to relatively large positive values (up to $\sim +18\,\mu$V/K) when Cr (2 to 7 at. %) is incorporated into Ni NWs. A pronounced drop of the thermopower with the impurity concentration was found in CoCr NW networks. Large thermoelectric power factors (in the range of 1–10 mW/K^2 m) were estimated on these magnetic NW networks, which holds promise for n- and p-type legs of flexible spin thermoelectric devices. The observed sign changes of the Seebeck coefficient and anisotropic magnetoresistance in NiCr and CoCr NW networks should be related to pronounced changes in the density of states for the majority spin electrons.

Financial support was provided by the Wallonia/Brussels Community (No. ARC 18/23-093) and the Belgian Fund for Scientific Research (FNRS). T. da C.S.C.G. is a Research Fellow of the FNRS. F.A.A. is a Postdoctoral Researcher of the FNRS. The authors would like to thank Dr. E. Ferain and the it4ip Company for supplying polycarbonate membranes.

REFERENCES

[1] I. Campbell and A. Fert, "Chapter 9 Transport properties of ferromagnets," *Handbook of Ferromagnetic Materials* (Elsevier, 1982), Vol. 3.
[2] J.-I. Inoue, "Chapter 2—gmr, tmr and bmr," in *Nanomagnetism and Spintronics*, edited by T. Shinjo (Elsevier, Amsterdam, 2009), pp. 15–92.
[3] H. C. Van Elst, "The anisotropy in the magneto-resistance of some nickel alloys," Physica **25**, 708–720 (1959).
[4] I. A. Campbell, A. Fert, and O. Jaoul, "The spontaneous resistivity anisotropy in ni-based alloys," J. Phys. C: Solid State Phys. **3**, S95 (1970).

[5]J. W. F. Dorleijn and A. R. Miedema, "An investigation of the resistivity anisotropy in nickel alloys," J. Phys. F: Met. Phys. **5**, 1543–1553 (1975).
[6]F. J. Blatt, P. A. Schroeder, C. L. Foiles, and D. Greig, *Thermoelectric Power of Metals* (Springer, Boston, MA, 1976).
[7]T. Farrell and D. Greig, "The thermoelectric power of nickel and its alloys," J. Phys. C: Solid State Phys. **3**, 138 (1970).
[8]M. C. Cadeville and J. Roussel, "Thermoelectric power and electronic structure of dilute alloys of nickel and cobalt with d transition elements," J. Phys. F: Met. Phys. **1**, 686 (1971).
[9]M. Hatami, G. E. W. Bauer, Q. Zhang, and P. J. Kelly, "Thermal spin-transfer torque in magnetoelectronic devices," Phys. Rev. Lett. **99**, 066603 (2007).
[10]K. Uchida, J. Xiao, H. Adachi, J. Ohe, S. Takahashi, J. Ieda, T. Ota, Y. Kajiwara, H. Umezawa, H. Kawai *et al.*, "Spin seebeck insulator," Nat. Mater. **9**, 894 (2010).
[11]G. E. W. Bauer, E. Saitoh, and B. J. van Wees, "Spin caloritronics," Nat. Mater. **11**, 391 (2012).
[12]A. Pushp, T. Phung, C. Rettner, B. P. Hughes, S.-H. Yang, and S. S. P. Parkin, "Giant thermal spin-torque–assisted magnetic tunnel junction switching," Proc. Natl. Acad. Sci. **112**, 6585–6590 (2015).
[13]S. R. Boona, R. C. Myers, and J. P. Heremans, "Spin caloritronics," Energy Environ. Sci. **7**, 885–910 (2014).
[14]K. Vandaele, S. J. Watzman, B. Flebus, A. Prakash, Y. Zheng, S. R. Boona, and J. P. Heremans, "Thermal spin transport and energy conversion," Mater. Today Phys. **1**, 39–49 (2017).
[15]J. He and T. M. Tritt, "Advances in thermoelectric materials research: Looking back and moving forward," Science **357**, eaak9997 (2017).
[16]J.-H. Bahk, H. Fang, K. Yazawa, and A. Shakouri, "Flexible thermoelectric materials and device optimization for wearable energy harvesting," J. Mater. Chem. C **3**, 10362–10374 (2015).
[17]Q. Zhang, Y. Sun, W. Xu, and D. Zhu, "Organic thermoelectric materials: Emerging green energy materials converting heat to electricity directly and efficiently," Adv. Mater. **26**, 6829–6851 (2014).
[18]Y. Du, J. Xu, B. Paul, and P. Eklund, "Flexible thermoelectric materials and devices," Appl. Mater. Today **12**, 366–388 (2018).
[19]T. da Câmara Santa Clara Gomes, F. Abreu Araujo, and L. Piraux, "Making flexible spin caloritronic devices with interconnected nanowire networks," Sci. Adv. **5**, eaav2782 (2019).
[20]F. Abreu Araujo, T. da Câmara Santa Clara Gomes, and L. Piraux, "Magnetic control of flexible thermoelectric devices based on macroscopic 3d interconnected nanowire networks," Adv. Electron. Mater. **5**, 1800819 (2019).
[21]A. Fert and L. Piraux, "Magnetic nanowires," J. Magn. Magn. Mater. **200**, 338–358 (1999).
[22]M. Staňo, O. Fruchart, and E. Brück, "Chapter 3—Magnetic nanowires and nanotubes," *Handbook of Magnetic Materials* (Elsevier, 2018), Vol. 27, pp. 155–267.
[23]T. Böhnert, V. Vega, A.-K. Michel, V. M. Prida, and K. Nielsch, "Magneto-thermopower and magnetoresistance of single co-ni alloy nanowires," Appl. Phys. Lett. **103**, 092407 (2013).
[24]O. Yamashita, S. Tomiyoshi, and K. Makita, "Bismuth telluride compounds with high thermoelectric figures of merit," J. Appl. Phys. **93**, 368–374 (2002).
[25]M. Rauber, I. Alber, S. Müller, R. Neumann, O. Picht, C. Roth, A. Schökel, M. E. Toimil-Molares, and W. Ensinger, "Highly-ordered supportless three-dimensional nanowire networks with tunable complexity and interwire connectivity for device integration," Nano Lett. **11**, 2304–2310 (2011).
[26]E. Araujo, A. Encinas, Y. G. Velázquez-Galván, J. M. Martínez-Huerta, G. Harmoir, E. Ferain, and L. Piraux, "Artificially modified magnetic anisotropy in interconnected nanowire networks," Nanoscale **7**, 1485–1490 (2015).
[27]E. Ferain and R. Legras, "Track-etch templates designed for micro- and nanofabrication," Nucl. Instrum. Methods Phys. Res., Sect. B **208**, 115–122 (2003).
[28]T. da Câmara Santa Clara Gomes, J. De La Torre Medina, Y. G. Velázquez-Galván, J. M. Martínez-Huerta, A. Encinas, and L. Piraux, "Interplay between the magnetic and magneto-transport properties of 3d interconnected nanowire networks," J. Appl. Phys. **120**, 043904 (2016).
[29]T. McGuire, J. Aboaf, and E. Klokholm, "Negative anisotropic magnetoresistance in 3d metals and alloys containing iridium," IEEE Trans. Magn. **20**, 972–974 (1984).
[30]O. Jaoul, I. Campbell, and A. Fert, "Spontaneous resistivity anisotropy in ni alloys," J. Magn. Magn. Mater. **5**, 23–34 (1977).
[31]J. Durand and F. Gautier, "Conduction a deux bandes et effet de periode dans les alliages a base de nickel et de cobalt," J. Phys. Chem. Solids **31**, 2773–2787 (1970).
[32]Y. D. Yao, S. Arajs, and E. E. Anderson, "Electrical resistivity of nickel-rich nickel-chromium alloys between 4 and 300 k," J. Low Temp. Phys. **21**, 369–376 (1975).
[33]S. R. Boona and D. T. Morelli, "Enhanced thermoelectric properties of $cepd_{3-x}pt_x$," Appl. Phys. Lett. **101**, 101909 (2012).